Article

Not peer-reviewed version

Investigating the Antifibrotic Effects of β-Citronellol on a TGF-β1-Stimulated LX-2 Hepatic Stellate Cell Model

Watunyoo Buakaew *, Sucheewin Krobthong, Yodying Yingchutrakul, Pachuen Potup, Yordhathai Thongsri, Krai Daowtak, Antonio Ferrante, Kanchana Usuwanthim *

Posted Date: 11 June 2024

doi: 10.20944/preprints202406.0645.v1

Keywords: β-citronellol; Citrus hystrix DC.; Hepatic stellate cell; Liver fibrosis; Proteomic analysis; Molecular docking

 doi:10.20944/preprints202406.0645.v1

Article

Investigating the Antifibrotic Effects of β-Citronellol on a TGF-β1-Stimulated LX-2 Hepatic Stellate Cell Model

Watunyoo Buakaew [1,2], Sucheewin Krobthong [3,4], Yodying Yingchutrakul [4], Pachuen Potup [2], Yordhathai Thongsri [2], Krai Daowtak [2], Antonio Ferrante [5,6] and Kanchana Usuwanthim [2,*]

[1] Department of Microbiology, Faculty of Medicine, Srinakharinwirot University, Bangkok, 10110, Thailand; watunyoo@g.swu.ac.th
[2] Cellular and Molecular Immunology Research Unit (CMIRU), Faculty of Allied Health Sciences, Naresuan University, Phitsanulok, 65000, Thailand; pachuenp@nu.ac.th
[3] Center of Excellence in Natural Products Chemistry (CENP), Department of Chemistry Faculty of Science, Chulalongkorn University, Bangkok, 10330, Thailand; sucheewin.k@chula.ac.th
[4] National Center for Genetic Engineering and Biotechnology, NSTDA, Pathum Thani, 12120, Thailand; yodying.yin@nstda.or.th
[5] Department of Immunopathology, South Australia (SA) Pathology, Women's and Children's Hospital, North Adelaide, SA, Australia; antonio.ferrante@adelaide.edu.au
[6] Department of Paediatrics, Adelaide School of Medicine, Department of Molecular and Biomedical Science, School of Biological Science and the Robinson Research Institute, University of Adelaide, South Australia 5000; antonio.ferrante@adelaide.edu.au
* Correspondence: kanchanau@nu.ac.th

Abstract: Liver fibrosis, a consequence of chronic liver damage or inflammation, is characterized by the excessive buildup of extracellular matrix components. This progressive condition significantly raises the risk of severe liver diseases like cirrhosis and hepatocellular carcinoma. The lack of approved therapeutics underscores the urgent need for novel anti-fibrotic drugs. Hepatic stellate cells (HSCs), key players in fibrogenesis, are promising targets for drug discovery. This study investigated the anti-fibrotic potential of *Citrus hystrix* DC. (KL) and its bioactive compound, β-citronellol (β-CIT), in a human HSC cell line (LX-2). Cells exposed to TGF-β1 to induce fibrogenesis were co-treated with crude KL extract and β-CIT. Gene expression was analyzed by Real-Time qRT-PCR to assess fibrosis-associated genes (*ACTA2*, *COL1A1*, *TIMP1*, *SMAD2*). The releasing of matrix metalloproteinase 9 (MMP-9) was measured by ELISA. Proteomic analysis and molecular docking identified potential signaling proteins and modeled protein-ligand interactions. Results showed that both crude KL extract and β-CIT suppressed HSC activation genes and MMP-9 levels. The MAPK signaling pathway emerged as a potential target of β-CIT. This study demonstrates the ability of KL extract and β-CIT to inhibit HSC activation during TGF-β1-induced fibrogenesis, suggesting a promising role of β-CIT in anti-hepatic fibrosis therapies.

Keywords: β-citronellol; *Citrus hystrix* DC.; Hepatic stellate cell; Liver fibrosis; Proteomic analysis; Molecular docking

1. Introduction

Liver disease accounts for 4% of all deaths worldwide, and the most common cause is cirrhosis [1]. Cirrhosis is an advanced stage of liver fibrosis, characterized by the irreversible formation of regenerative nodules with excessive extracellular matrix (ECM) accumulation. Liver fibrogenesis is the key mechanism in the wound-healing process of the liver after inflammation and injury, providing fibril-forming collagen as a scaffold for tissue regeneration [2]. Various intrinsic and extrinsic stimuli of hepatic inflammation, such as cholecystitis, viral hepatitis, alcohol consumption, and non-alcoholic fatty liver disease (NAFLD), lead to the activation of hepatic stellate cells (HSCs)

 doi:10.20944/preprints202406.0645.v1

[3]. HSCs differentiate from myofibroblasts and have been established as the central driver of liver fibrogenesis in *in vitro* and *in vivo* experiments [4]. In the homeostasis of the wound healing process, ECM deposition is a tightly regulated process that is reversible after the stimulant is removed. Transforming growth factor-beta 1 (TGF-β1) is a one of key molecules involved in liver fibrogenesis in HSCs via the stimulation of mothers against decapentaplegic homolog (SMAD) transcription factors [4]. Patients with chronic liver fibrosis progression are at a higher risk of developing liver cancer such as hepatocellular carcinoma (HCC) [5]. At present, there is no standard treatment available for liver fibrosis [6], and novel approaches to treat this condition is a sort-after-goal. Therefore, finding a novel and effective treatment could explore the possibility of a therapeutic approach.

Citrus hystrix DC., also known as Kaffir lime (KL), is a plant belonging to the Rutaceae family that is cultivated mainly in Asiatic countries. The KL is well-known as the source of unique volatile compounds in an ingredient of foods and alternative medicine. Several chemical compounds are responsible for an intense kaffir lemon odor, such as Citronellal, L-Linalool, 1,8-Cineole, and α-Terpeneol [7]. The extract and active compounds from this plant harbor several pharmacological activities, including anti-inflammatory [8,9], antioxidants [10,11], anti-microbial [12,13], and anti-cancer effects [14–16]. The hepatoprotective effects of KL have been reported in paracetamol-induced liver injury in mice models [17]. However, the anti-liver fibrosis activity of the KL extract and its derivative compounds remains unexplored.

In this study, we examined the anti-fibrotic effects of the crude extract and β-citronellol, an active compound identified from the KL leaf. β-citronellol is a monoterpenoid that has been previously reported with anti-inflammatory, anti-fungal, and anti-cancer properties [9,15,18]. The anti-liver fibrosis activity of β-citronellol was tested in TGF-β1-induced human HSCs (LX-2 cells). Several hepatic fibrogenesis markers were measured, including genes and protein of HSCs. Proteomics and molecular docking analyses were employed to elucidate the possible β-citronellol mechanisms of action on LX-2 cells. Our study suggested the potential role of KL extract and its compound in preventing liver fibrosis development in the HSCs model, providing a new source for anti-hepatic fibrosis research.

2. Materials and Methods

2.1. Preparation of crude extract and active compound

The initial crude extract of KL leaves employed in this investigation was generated via maceration of KL powder, as detailed in a prior publication [9]. Briefly, a 1,000-gram sample of KL powder underwent sequential maceration in *n*-hexane (absolute), ethyl acetate (95%), and ethanol (95%) for periods of three days each. Following filtration and evaporation of the ethanolic solute, 100.56 grams of crude ethanolic KL leaf extract were obtained. The active compound β-citronellol was acquired from a commercial chemical supplier. Stock solutions of both the crude extract and the active compound were formulated using a solvent mixture of DMSO and Tween-80 (1:1 ratio). Throughout cell treatment procedures, residual solvent concentration was maintained below 0.5%.

2.2. Cell culture

LX-2 cells (an immortalized human hepatic stellate cell line) were cultured in Dulbecco's Modified Eagle Medium (DMEM) supplemented with 2% fetal bovine serum (FBS) and 1% antibiotic-antimycotic solution. The cells were maintained in a humidified incubator at 37°C with 5% CO_2. This cell line was kindly provided by Dr. Saranyapin Potikanond (Department of Pharmacology, Chiang Mai University, Thailand).

 doi:10.20944/preprints202406.0645.v1

2.3. Cell viability assay

To establish the optimal treatment concentrations of crude Kaffir lime leaf extract (KL) and β-citronellol (β-CIT) on LX-2 cells, a resazurin reduction cytotoxicity assay was conducted. LX-2 cells were seeded (2×10^4 cells/well) in a 96-well plate and treated with varying concentrations of KL and β-CIT (0 – 1,000 µg/mL). Following a 24 h incubation at 37°C, resazurin (25 µg/mL) was added, and fluorescence was measured after 4 h (excitation/emission: 560/590 nm) using an EnSpire® Multimode microplate reader. GraphPad Prism version 8 (GraphPad Software, La Jolla, CA, USA) was used to determine inhibitory concentrations (IC). The IC_{10} value was selected as the maximum safe concentration for further experimental use.

2.4. RNA extraction and gene expression analysis

To assess the potential anti-fibrotic effects of KL and β-CIT on gene expression, LX-2 cells (2×10^5 cells/well) were seeded into 24-well plates and stimulated with TGF-β1 (10 ng/mL) to induce fibrogenesis. Following this, the cells were treated with selected concentrations of both compounds and incubated for 24 hours. After the treatment period, the supernatant was discarded, and RNA extraction was performed using Trizol reagent in adherence to the manufacturer's instructions. RNA concentration and purity were assessed utilizing a Nanodrop spectrophotometer. Subsequently, cDNA synthesis was performed on the extracted RNA from each condition using a Tetro™ cDNA Synthesis Kit. Quantitative real-time polymerase chain reaction (real time qPCR) was employed to evaluate the expression levels of genes implicated in liver fibrosis. Amplification of gene transcripts was achieved using nucleotide primers designed specifically for *ACTA2*, *TIMP1*, *COL1A1*, and *SMAD2* genes. The qPCR reactions were carried out with a SensiFAST™ SYBR® No-ROX Kit on a CFX96 Touch Real-Time PCR Detection System (Bio-Rad Laboratories, Hercules, CA, USA). The PCR protocol consisted of an initial polymerase activation step (95°C, 1 min), followed by 45 cycles comprising denaturation (95°C, 10 s) and annealing/extension (60°C, 1 min). The $2^{(-\Delta\Delta Ct)}$ [19] method was used to determine the relative expression of each target gene, normalized against the internal reference gene, *GAPDH*. Table 1 provides a comprehensive list of the forward and reverse primers used for each gene [20].

Table 1. The PCR primer of each gene in this study.

Gene	Description	Forward primer (3′ → 5′)	Reverse primer (3′ → 5′)
ACTA2	actin alpha 2, smooth muscle	CATCCTCATCCTCCCTTGAG	ATGAAGGATGGCTGGAACAG
COL1A1	Collagen type I alpha 1 chain	CCGGCTCCTGCTCCTCTTAGCG	CGTTCTGTACGCAGGTGATTGGTGG
TIMP1	TIMP metallopeptidase inhibitor 1	CAAGATGTATAAAGGGTTCCAAGC	TCCATCCTGCAGTTTTCCAG
SMAD2	SMAD family member 2	TGCTCTGAAATTTGGGGACTGA	GACGACCATCAAGAGACCTGG
GAPDH	Glyceraldehyde-3-phosphate dehydrogenase	ATGACATCAAGAAGGTGGTG	CATACCAGGAAATGAGCTTG

2.5. Measurement of the MMP-9 production

The activation of hepatic stellate cells (HSCs) is characterized by the release of matrix metalloproteinase 9 (MMP-9), a pivotal enzyme in this process. To assess whether KL and β-CIT exhibit MMP-9 inhibitory activity, LX-2 cells (2×10^5 cells/well) were seeded in 24-well plates and stimulated with TGF-β1 (10 ng/mL), either alone or in conjunction with KL and β-CIT, for 24 hours. Quantification of MMP-9 in the collected supernatants was performed using a human MMP-9 ELISA

 doi:10.20944/preprints202406.0645.v1

kit, adhering to the manufacturer's protocol. Absorbance readings were analyzed using GraphPad Prism version 8 to determine MMP-9 levels.

2.6. LC-MS/MS analysis

2.6.1. Preparation of protein sample

To rigorously assess the impact of KL and β-CIT on TGF-β1-induced LX-2 cell global protein expression, liquid chromatography with tandem mass spectrometry (LC-MS/MS) was employed. Cellular treatment and lysate extraction procedures were consistent with those outlined in the previous section. LC-MS/MS sample preparation followed an established protocol with minor adjustments to ensure analytical reproducibility [21]. Protein concentration was attained through the use of a 3 kDa molecular weight cut-off filter. Subsequent precipitation was induced with ice-cold acetone (1:5 v/v). The resulting pellet was then resuspended in a solution of 0.3% RapidGest SF and 2.5 mM ammonium bicarbonate. A 30-μg protein aliquot was subjected to tryptic digestion. To facilitate proteolysis, disulfide bonds were reduced with 1 mM tris(2-carboxyethyl) phosphine (TCEP) at 37 °C for 2 hours, followed by alkylation with 5 mM iodoacetamide (IAA) at room temperature for 50 minutes in a light-protected environment. The sample underwent desalting (Zeba Spin Column) before a second tryptic digestion step (1:40 enzyme-protein ratio) at 37 °C for 6 hours. Finally, the digested peptides were dried and resuspended in 0.1% formic acid in preparation for LC-MS/MS analysis.

2.6.2. Proteomic data analysis

Protein samples underwent analytical scrutiny via a high-fidelity hybrid Quadrupole-Orbitrap system (HF-X) coupled with an EASY-nLC1000 for refined separation. A nano C18 column operating in positive ionization mode facilitated chromatographic resolution. Employing a calibrated gradient of 90% acetonitrile/0.1% formic acid over 135 minutes (300 nL/min), with mobile phase A consisting of 0.1% formic acid in water, optimal separation was achieved. The column was meticulously regenerated and re-equilibrated. Data-dependent acquisition (TopN15) utilizing higher-energy collisional dissociation (29 eV) directed peptide analysis. Proteome Discoverer™ 2.4 software integrated MS parameters and thorough database searches (UniProt Homo sapiens, 14/01/2023). Stringent peptide/protein tolerances, modifications, and a 1% FDR ensured data integrity. After normalization (total intensity count), pathway analysis employed PADOG within Reactome v84 (Homo sapiens, 25/02/2023) [22].

2.7. Molecular docking analysis

Computational molecular docking analysis was performed to investigate the interaction between β-CIT and selected proteins implicated in HSCs activation, a key process in liver fibrosis. Protein 3D structures associated with HSC activation during hepatic fibrosis were obtained from the RCSB Protein Data Bank (RCSB PDB) [23,24] and prepared in PDB format. The chemical structure of β-citronellol (PubChem CID 8842) was retrieved from PubChem [25]. The protein-ligand blind docking analysis was conducted using the CB-Dock2 server (https://cadd.labshare.cn/cb-dock2/index.php) [26]. Prior to docking analysis, both the protein targets and β-citronellol were prepared using the DockPrep tool within UCSF Chimera alpha software version 1.18 [27]. Post-docking, interactions between the target proteins and ligand were visualized in 2D using BIOVIA Discovery Studio Visualizer version 21.1.0.20298 (San Diego, USA).

 doi:10.20944/preprints202406.0645.v1

2.8. Statistical analysis

Each *in vitro* experimental procedure was conducted in triplicate. Unless otherwise specified, data representation follows a mean ± SD format. Statistical significance between means was assessed using one-way ANOVA (Tukey's multiple comparison test) within GraphPad Prism software (version 8.0.1). A *p*-value threshold of < 0.05 denoted statistical significance.

3. Results

3.1. Cytotoxicity of crude extract and active compound on the LX-2 cell line

The cytotoxic potential of crude KL extract and its constituent compound, β-CIT, was assessed on the LX-2 cell line through the resazurin reduction assay. Dose-response curves were generated to determine IC_5, IC_{10}, and IC_{50} values. Results demonstrated that the crude extract exhibited lower cytotoxicity relative to β-CIT, yielding IC_{50} values of 351.80 µg/mL and 18.72 µg/mL respectively (Figure 1). Furthermore, crude KL extract displayed IC_5 and IC_{10} values of 96.03 µg/mL and 133.48 µg/mL, while β-CIT exhibited notably lower values of 0.66 µg/mL and 1.54 µg/mL. Based on these findings, subsequent experiments investigating effects on LX-2 cells were conducted using maximum concentrations of 120 µg/mL for the crude extract and 1 µg/mL for β-CIT.

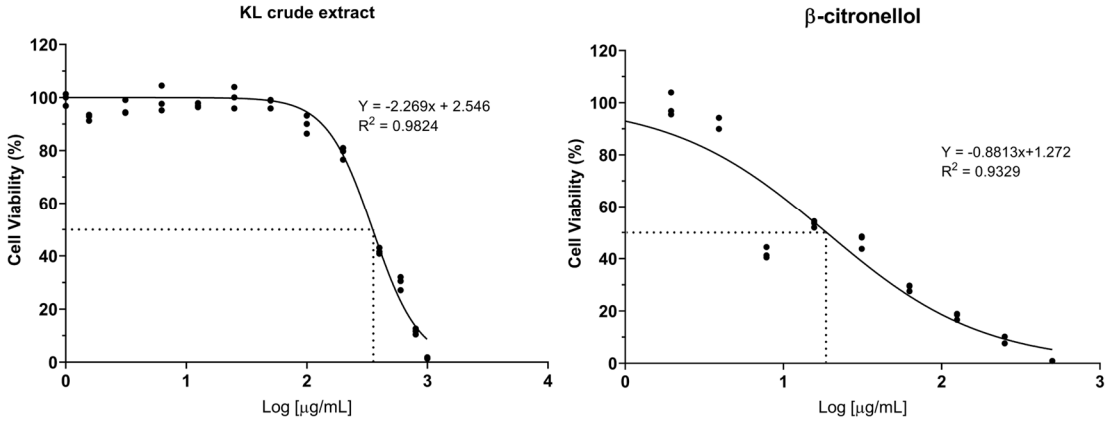

Figure 1. Dose-response curve of crude KL extract and β-citronellol on viability of the LX-2 cells.

3.2. The inhibition of activated HSCs genes expression and MMP-9 production

Quantitative real-time polymerase chain reaction (qRT-PCR) elucidated downregulation of key hepatic fibrosis markers (*ACTA2*, *COL1A1*, and *SMAD2*) upon exposure to crude KL extract. Similarly, β-CIT treatment demonstrated inhibition of *ACTA2*, *COL1A1*, and *TIMP1* gene expression. Analysis of MMP-9 levels via the ELISA kit revealed a marked, dose-dependent reduction following exposure to crude KL extract, with a comparable decrease observed with β-CIT treatment. These findings collectively point towards antifibrotic potential in both compounds, as evidenced by their capacity to attenuate TGF-β1-induced fibrogenesis in the LX-2 cell model.

 doi:10.20944/preprints202406.0645.v1

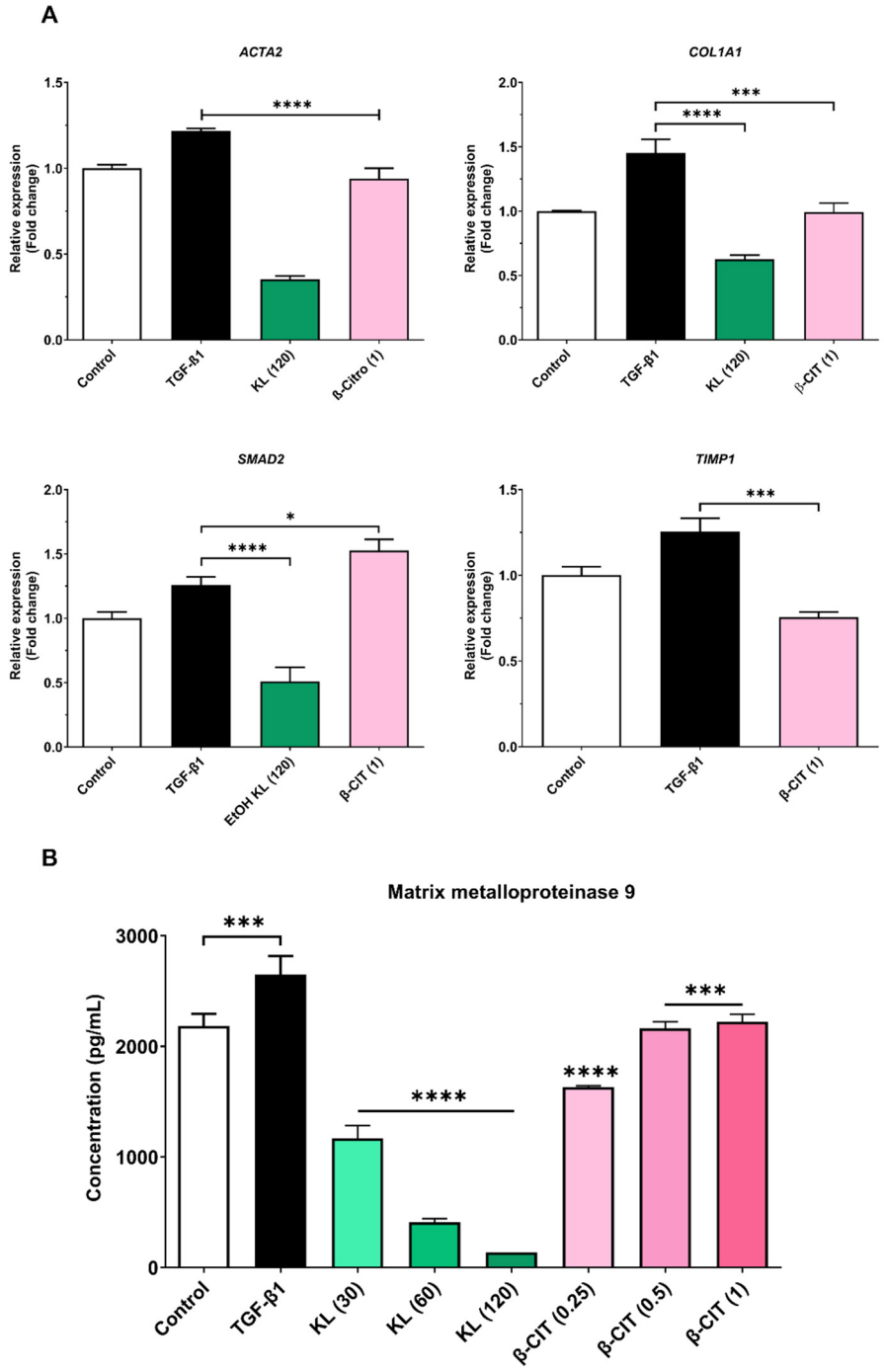

Figure 2. Crude KL extract and β-CIT attenuate the expression of hepatic fibrosis-associated genes and mitigate MMP-9 production in LX-2 cells challenged with TGF-β1. Following a 24-hour co-treatment protocol, mRNA was extracted and subjected to real-time qRT-PCR analysis. Expression levels were normalized to the housekeeping gene *GAPDH* (A), revealing a marked downregulation of fibrosis-related genes. Furthermore, a statistically significant reduction in MMP-9 levels was observed in the cell culture supernatant (B). Statistical significance was denoted as follows: $p < 0.0332$ (*), $p < 0.0021$ (**), $p < 0.0002$ (***), $p < 0.0001$ (****).

3.3. Proteomic analysis of the effect of β-citronellol on LX-2 cell

To elucidate the impact of β-CIT on TGF-β1-induced LX-2 cells, a 48-hour treatment regimen with β-CIT was implemented. Subsequent protein extraction and LC-MS/MS analysis yielded a total of 1,570 overlapping proteins present in both TGF-β1 treatment alone and β-CIT co-treatment

 doi:10.20944/preprints202406.0645.v1

conditions (Figure 3A). Rigorous filtering parameters were applied (log2 fold change of ±1.5 and *p*-value < 0.05) resulting in the identification of 125 upregulated and 65 downregulated proteins (Figure 3B). The list of DEPs was summarized in Table 2. Further analysis of these differentially expressed proteins (DEPs) was conducted utilizing protein-protein interaction (PPI) network visualization, revealing intricate relationships among the DEPs (Figure 3C,D).

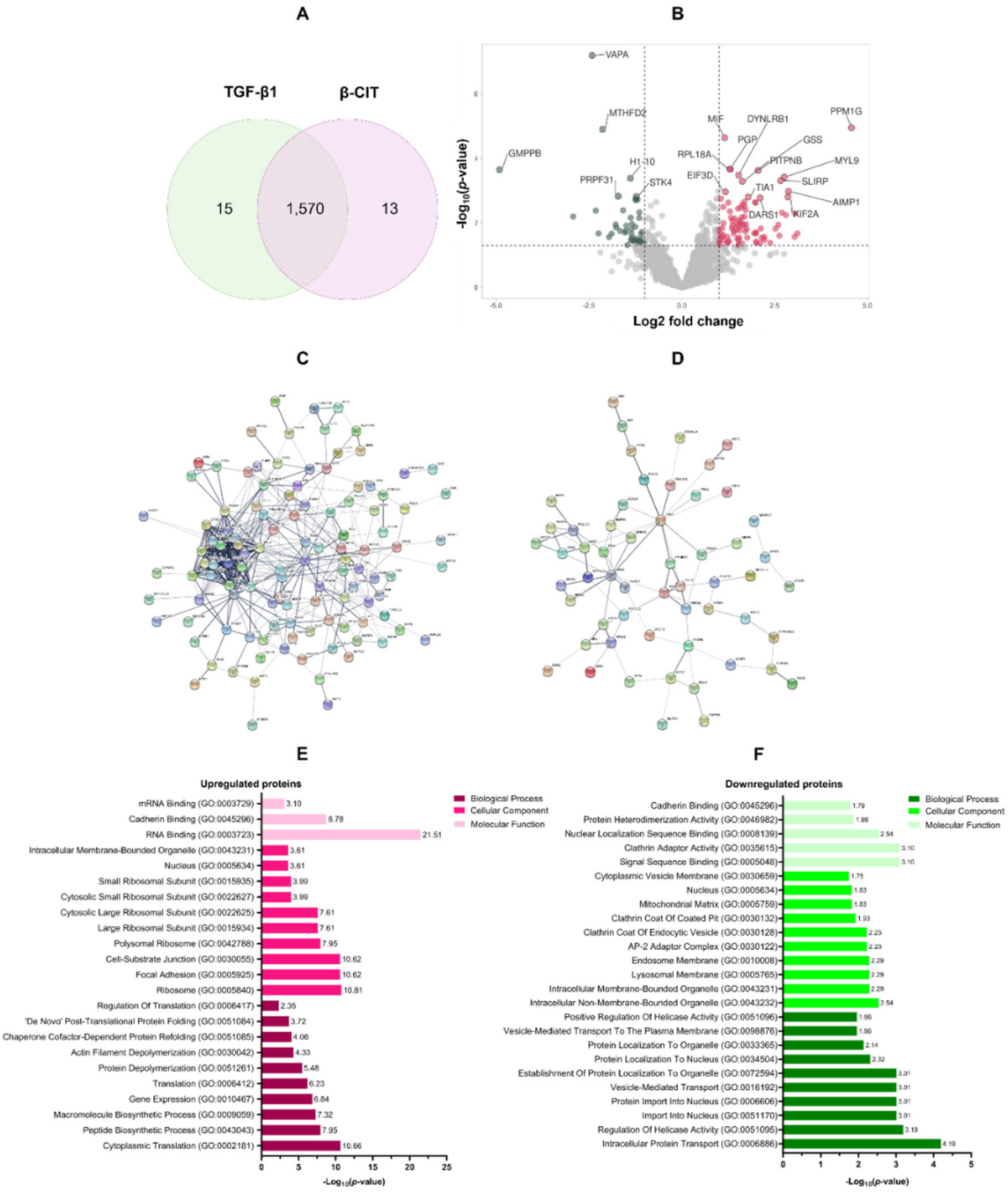

Figure 3. The functional enrichment analysis of DEPs. Quantitative LC-MS/MS analysis yielded a total of 1,570 differentially expressed proteins (DEPs) (A). Volcano plots visually demonstrated the upregulated (n=125, red) and downregulated (n=65, green) proteins within this dataset (B). To elucidate potential functional relationships, protein-protein interaction (PPI) network analyses were performed separately for the upregulated (C) and downregulated (D) protein subsets. Gene Ontology (GO) annotations illuminated key biological processes associated with both upregulated (E) and downregulated (F) DEPs.

 doi:10.20944/preprints202406.0645.v1

Table 2. The top-10 expression proteins in both upregulated and downregulated manners.

Uniprot ID	Gene ID	Description	Log2 fold change	-Log10 *p*-value
Top-10 upregulated proteins				
O15355	*PPM1G*	Protein phosphatase, Mg2+/Mn2+ dependent 1G	4.57	4.95
Q9Y4W6	*AFG3L2*	AFG3-like protein 2	3.11	1.68
P04066	*FUCA1*	Tissue alpha-L-fucosidase	3.05	2.29
Q16537	*PPP2R5E*	Serine/threonine-protein phosphatase 2A 56 kDa regulatory subunit epsilon isoform	3.04	1.57
Q12904	*AIMP1*	Aminoacyl tRNA synthase complex-interacting multifunctional protein 1	2.87	2.98
O00139	*KIF2A*	Kinesin-like protein KIF2A	2.85	2.80
Q16186	*ADRM1*	Proteasomal ubiquitin receptor ADRM1	2.80	2.24
P24844	*MYL9*	Myosin regulatory light polypeptide 9	2.76	3.42
Q0VDF9	*HSPA14*	Heat shock 70 kDa protein 14	2.69	2.32
Q9GZT3	*SLIRP*	SRA stem-loop-interacting RNA-binding protein, mitochondrial	2.66	3.31
Top-10 downregulated proteins				
Q9Y5P6	*GMPPB*	Mannose-1-phosphate guanyltransferase beta	-4.91	3.65
O75431	*MTX2*	Metaxin-2	-2.92	2.20
Q9P0L0	*VAPA*	Vesicle-associated membrane protein-associated protein A	-2.42	7.19
P04264	*KRT1*	Keratin, type II cytoskeletal 1	-2.32	2.38
O76021	*RSL1D1*	Ribosomal L1 domain-containing protein 1	-2.24	1.67
P13995	*MTHFD2*	Bifunctional methylenetetrahydrofolate dehydrogenase/cyclohydrolase, mitochondrial	-2.14	4.90
P51398	*DAP3*	28S ribosomal protein S29, mitochondrial	-1.96	1.56
Q9P2R3	*ANKFY1*	Rabankyrin-5	-1.89	1.66
O00291	*HIP1*	Huntingtin-interacting protein 1	-1.78	1.95

Gene ontology (GO) annotation of differentially expressed proteins (DEPs) revealed distinct functional profiles for those exhibiting upregulation versus downregulation. Biological process enrichment demonstrated a clear emphasis on protein synthesis within the upregulated group, including cytoplasmic translation (GO:0002181), peptide biosynthesis (GO:0043043), macromolecule biosynthesis (GO:0009059), gene expression (GO:0010467), and overall translation (GO:0006412). Conversely, downregulated proteins displayed association with processes governing intracellular transport (GO:0006886), helicase regulation (GO:0051095), nuclear import (GO:0051170 & GO:0006606), and vesicle-based transport (GO:0016192). Cellular component analysis further elucidated this contrast. Upregulated proteins were overrepresented in ribosomal structures (GO:0005840, GO:0042788, GO:0015934), alongside focal adhesions (GO:0005925) and cell-substrate junctions (GO:0030055). Downregulated proteins were preferentially associated with both membrane-bound (GO:0043231) and non-membrane-bound (GO:0043232) intracellular organelles, as well as components of the lysosomal (GO:0005765), endosomal (GO:0010008), and AP-2 adaptor complex (GO:0030122). Molecular function categories mirrored these distinctions. Upregulated proteins exhibited enrichment for various RNA binding functions (GO:0003723, GO:0003729), cadherin binding (GO:0045296), signal sequence binding (GO:0005048), and activities related to clathrin adaptor function (GO:0035615). Downregulation encompassed proteins involved in nuclear localization sequence binding (GO:0008139), protein heterodimerization (GO:0046982), and cadherin binding (GO:0045296). These findings are summarized in Figure 3E,F.

KEGG pathway enrichment analysis was conducted to identify signaling cascades potentially modulated by β-citronellol treatment in LX-2 cells. Enriched pathways included those associated with ribosome function, coronavirus disease, Salmonella infection, Parkinson's disease, and

 doi:10.20944/preprints202406.0645.v1

spinocerebellar ataxia (Figure 4A). Downregulated proteins showed significant involvement in Huntington's disease, Vibrio cholerae infection, endocrine-regulated calcium reabsorption, phagosome formation, and synaptic vesicle cycling (Figure 4B). The MAPK signaling pathway (Figure 4C), a known contributor to hepatic fibrosis, was a focus of further examination, with downregulated proteins highlighted in blue.

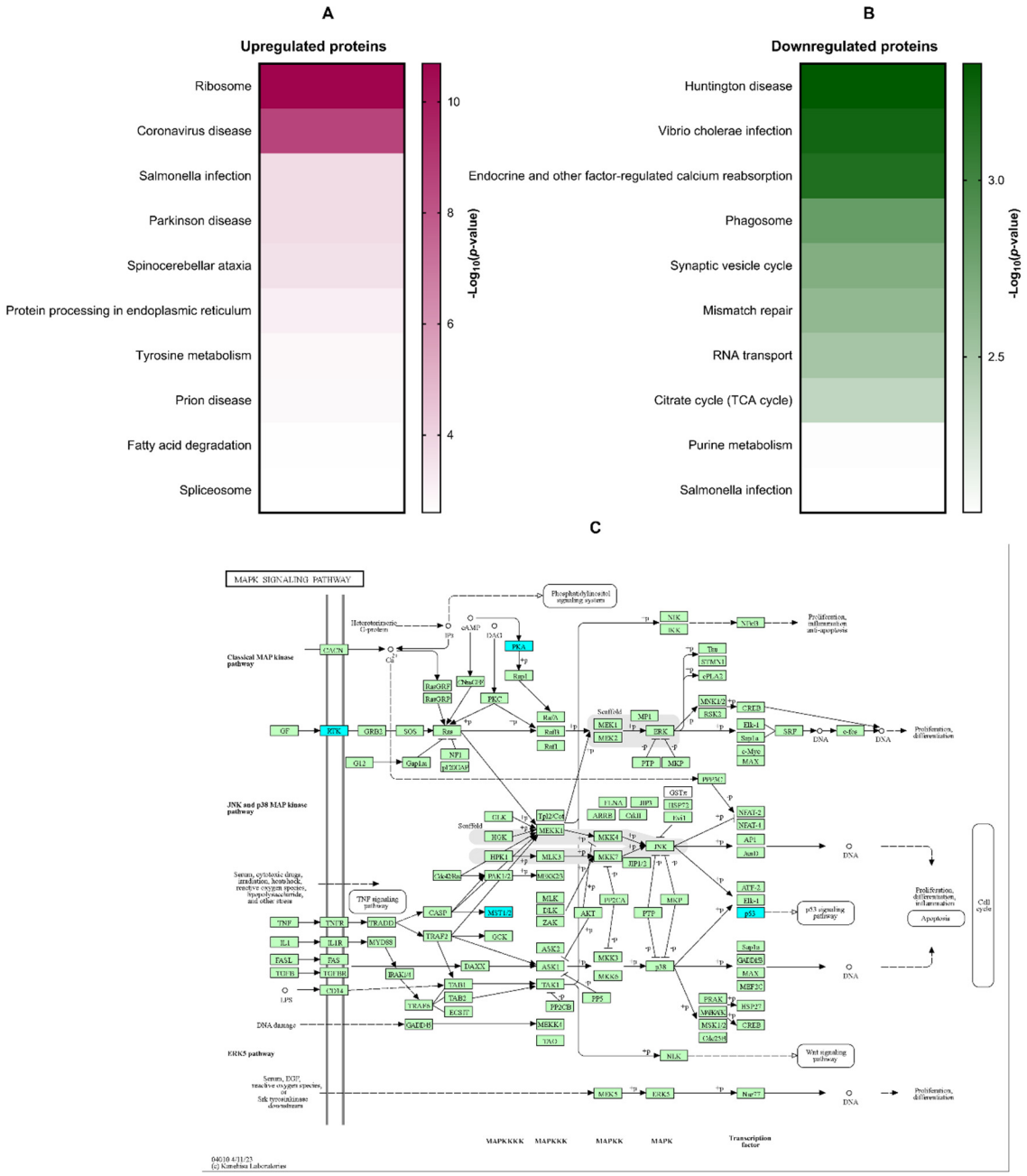

Figure 4. The KEGG analysis of DEPs. Amongst the most significantly enriched KEGG signaling pathways, differential protein expression patterns emerged (upregulated: A; downregulated: B). Notably, the MAPK signaling pathway exhibited a pronounced association with downregulated proteins (C; indicated in blue). .

3.4. In silico molecular docking analysis

Binding interactions between β-citronellol and potential protein targets were examined using the cavity detection-guided blind docking capabilities of the CB-Dock2 web-based platform. Detailed results, including Autodock Vina binding scores and the amino acids involved in the interactions, are outlined in Table 3. Visualization of the protein-ligand interactions in 2D and 3D formats can be

Preprints.org (www.preprints.org) | NOT PEER-REVIEWED | Posted: 11 June 2024 doi:10.20944/preprints202406.0645.v1

found in Figure 5. Of particular interest, β-citronellol displayed favorable binding scores (-4 to -6 Kcal/mol) with target proteins known to participate in the MAPK signaling pathway.

Table 3. The Autodock Vina binding score and interaction amino acid of seleted proteins.

PDB ID	Protein name	Binding score (Kcal/mol)	Interacting amino acid
1MQB	Ephrin type-A receptor 2	-5.0	Ile619, Val627, Ala644, Lys646, Glu663, Tyr694, Met695, Leu746, Ser756
7Y1G	cAMP-dependent protein kinase catalytic subunit alpha	-5.4	Phe129, Lys168, Pro169, Glu203, Phe239
8FMI	GTPase KRas	-4.8	Val7, Asp54, Leu56, Tyr71
1C1Y	RAF proto-oncogene serine/threonine-protein kinase	-4.2	His79, Lys84, Leu86, Lys87, Pro93
1S9J	Dual specificity mitogen-activated protein kinase kinase 1	-5.3	Leu74, Val82, Ala95, Met143, Asn195, Leu197, Cys207
2ZOQ	Mitogen-activated protein kinase 3	-5.7	Leu86, Arg87, Arg189, Ile190, Phe348, Leu352

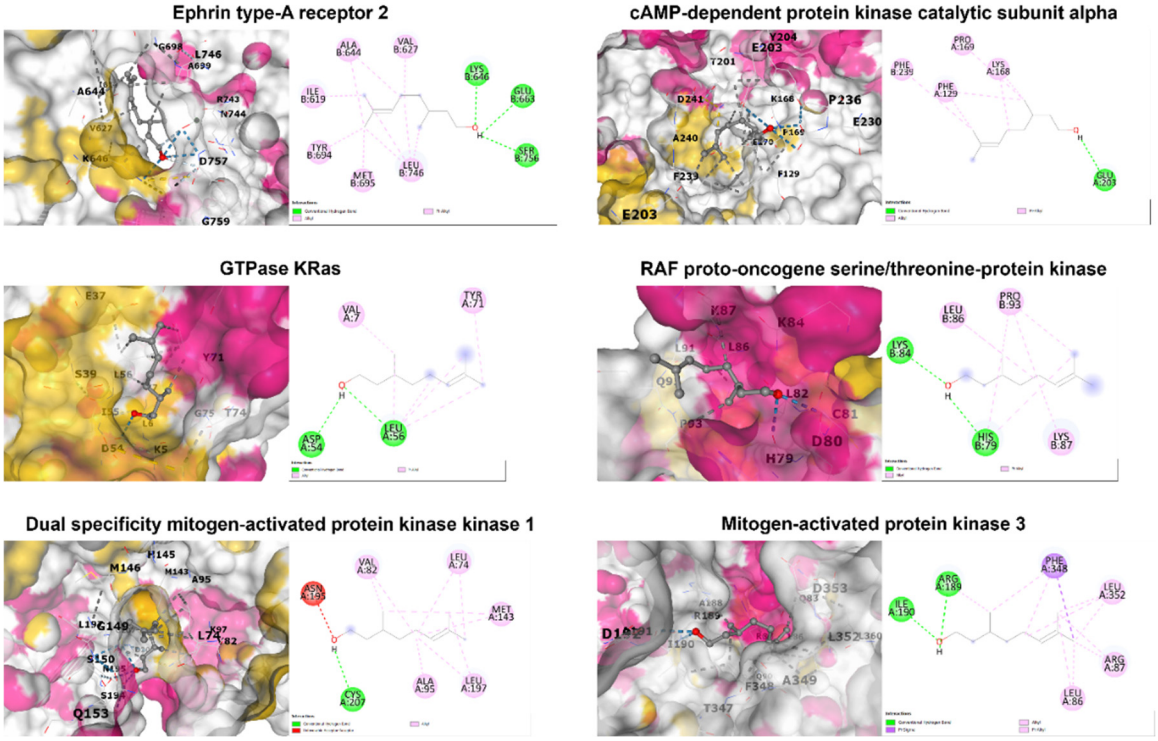

Figure 5. The 2D and 3D structures of candidate target proteins and β-CIT interaction.

4. Discussion

Considered the antecedent stage of irreversible cirrhosis, liver fibrosis arises from sustained liver injury and predisposes individuals to grave complications such as portal hypertension, hepatic encephalopathy, and hepatocellular carcinoma. The asymptomatic presentation of hepatic fibrosis, coupled with diagnostic challenges, frequently allows for unchecked progression, even though the condition may be reversible upon removal of causative factors. Furthermore, the lack of a singular, targeted medication for liver fibrosis highlights the critical need for continued research in the development of effective anti-fibrotic agents.

 doi:10.20944/preprints202406.0645.v1

Hepatic stellate cell (HSC) activation is a pivotal factor in the pathogenesis of liver fibrosis. Transforming growth factor beta-1 (TGF-β1) serves as a highly effective activator of hepatic stellate cells (HSCs) via dual signaling mechanisms: the canonical (Smad-dependent) pathway and the non-canonical (non-Smad) pathway. The TGF-β1/Smad signaling cascade represents a well-documented process central to HSC activation during liver damage. Upon binding to its specific receptor, TGF-β type II receptor (TβRII), TGF-β1 initiates the recruitment of the TGF-β type I receptor (TβRI). TβRII subsequently activates TβRI through phosphorylation of serine residue, facilitating the phosphorylation of substrates like Smad2 and Smad3. Phosphorylated Smad2 and Smad3 then complex with Smad4, translocating into the nucleus. This Smad2/3/4 complex directly interacts with DNA, modulating the expression of key genes such as *ACTA2*, *COL1A1*, and *TIMP1* [28]. Our findings demonstrate that treatment of HSCs with crude KL extract and β-CIT effectively attenuates the transcriptional expression of these markers, implying a direct interference with the canonical pathway of TGF-β1-driven signaling cascade.

Proteomic analysis elucidated proteins and signaling pathways potentially mediating inhibitory effect of β-CIT on TGF-β1-induced HSCs. The KEGG database identified several signaling pathway, especially the downregulated pathways, including ribosome function, coronavirus disease, Salmonella infection, Parkinson's disease, and spinocerebellar ataxia. The mitogen-activated protein kinase (MAPK) signaling pathway is one of the non-canonical pathways in the HSC activation by the TGF-β1 [29]. The MAPK pathway is known to regulate diverse cellular functions such as proliferation, differentiation, survival, apoptosis, and inflammation. This pathway comprises three signaling cascades: ERK, JNK, and p38. Extensive research implicates this pathway in hepatic fibrosis through its influence on HSC behavior. MAPK signaling modulates proliferation, migration, and ECM synthesis/deposition following stimulation by growth factors like TGF-β1 via tyrosine kinases (RTKs) [30]. Our proteomic analysis demonstrated downregulation of the RTK proteins, Eph receptor A2 (*EPHA2*), alongside the MAPK signaling proteins kinase cAMP-activated catalytic subunit alpha (*PRKACA*). The Eph receptors are the largest known receptor tyrosine kinases in mammals, regulating vast biological activity of the cells, including cell adhesion, migration, proliferation, and immune cell activation [31]. The expression of Eph receptors has been linked to the progression of liver fibrosis [32]. *PRKACA* is a member of the PKA family, has a role to transfer phosphate groups to serine or threonine residues on substrate proteins, which can alter their function and activity. It is involved in various cellular processes, including metabolism, gene expression, and cell proliferation. Some studies have revealed that *PRKACA* exhibits hyperkinase activity in fibrotic liver samples from both humans and mice. This suggests that *PRKACA* may play a significant role in the development and progression of hepatic fibrosis [33]. Molecular binding analysis indicated favorable affinities between these proteins and β-CIT. These findings suggest anti-hepatic fibrosis potential of β-CIT may involve targeting the MAPK signaling pathway, though further studies are necessary to confirm the precise mechanism.

5. Conclusions

This study presents the first evidence of the potential anti-hepatic fibrotic activity of β-CIT. We demonstrate that β-CIT inhibits hepatic stellate cell activation induced by the TGF-β1 model. Mechanistically, β-CIT appears to target the canonical TGF-β1/Smad signaling pathway, along with reducing MMP-9 production—all major contributors to extracellular matrix (ECM) deposition. Further proteomic analysis and molecular docking suggest a potential additional mode of action involving MAPK tyrosine kinase signaling proteins. While *in vitro* results are promising, further in vivo investigations are required to fully understand therapeutic potential of β-CIT for liver fibrosis.

Author Contributions: This research was contributed by authors "conceptualization, K.U. and W.B.; methodology, W.B.; formal analysis, W.B., S.K. and Y.Y; investigation, W.B.; resources, P.P., and K.D.; data curation, K.U., and Y.T.; writing—original draft preparation, W.B.; writing—review and editing, W.B., A.F. and K.U.; visualization, K.U. and W.B.; supervision, K.U.; funding acquisition, K.U. All authors have read and agreed to the published version of the manuscript.

 doi:10.20944/preprints202406.0645.v1

Funding: This work was support by Thailand Science Research and Innovation, and Naresuan University (R2567B041) and "the APC was funded by Reinventing University Program 2023, The Ministry of Higher Education, Science, Research and Innovation (MHESI), Thailand (R2566A056).

Institutional Review Board Statement: The study was conducted in accordance with the Declaration of Helsinki and approved by the Institutional Review Board of Naresuan University (IRB No. P1-0133/2565, approved on October 21, 2022).

Informed Consent Statement: Not applicable.

Data Availability Statement: The original data presented in the study are openly available in ProteomeXchange Consortium via the PRIDE partner repository at http://www.ebi.ac.uk/pride/archive/, PXD052806. The following username and password can be used to access the dataset by logging in to the PRIDE website.

Username: reviewer_pxd052806@ebi.ac.uk
Password: 24jgZXwu1IAN

Acknowledgments: The authors gratefully acknowledge Associate Professor Dr. Saranyapin Potikanond (Department of Pharmacology, Faculty of Medicine, Chiang Mai University) for the generous contribution of the LX-2 cells used in this research.

Conflicts of Interest: The funders had no role in the design of the study; in the collection, analyses, or interpretation of data; in the writing of the manuscript; or in the decision to publish the results.

References

1. Devarbhavi, H.; Asrani, S.K.; Arab, J.P.; Nartey, Y.A.; Pose, E.; Kamath, P.S. Global burden of liver disease: 2023 update. *J Hepatol* **2023**, *79*, 516-537.
2. Luangmonkong, T.; Parichatikanond, W.; Olinga, P. Targeting collagen homeostasis for the treatment of liver fibrosis: Opportunities and challenges. *Biochem Pharmacol* **2023**, *215*, 115740.
3. Acharya, P.; Chouhan, K.; Weiskirchen, S.; Weiskirchen, R. Cellular Mechanisms of Liver Fibrosis. *Front Pharmacol* **2021**, *12*, 671640.
4. Tsuchida, T.; Friedman, S.L. Mechanisms of hepatic stellate cell activation. *Nat Rev Gastroenterol Hepatol* **2017**, *14*, 397-411.
5. Dhar, D.; Baglieri, J.; Kisseleva, T.; Brenner, D.A. Mechanisms of liver fibrosis and its role in liver cancer. *Exp Biol Med (Maywood)* **2020**, *245*, 96-108.
6. Zhang, C.Y., Liu, S., & Yang, M. Treatment of liver fibrosis: Past, current, and future. *World J Hepatol* **2023**, *15*, 755–774.
7. Agouillal, F.; Taher, Z.; Moghrani, H.; Nasrallah, N.; El Enshasy, H. A Review of Genetic Taxonomy, Biomolecules Chemistry and Bioactivities of Citrus hystrix DC. *Biosci Biotechnol Res Asia* **2017**, *14*, 285-305.
8. Kidarn, S.; Saenjum, C.; Hongwiset, D.; Phrutivorapongkul, A. Furanocoumarins from Kaffir lime and their inhibitory effects on inflammatory mediator production. *Cogent Chem* **2018**, *4*, 1529259.
9. Buakaew, W.; Pankla Sranujit, R.; Noysang, C.; Thongsri, Y.; Potup, P.; Nuengchamnong, N.; Suphrom, N.; Usuwanthim, K. Phytochemical Constituents of *Citrus hystrix* DC. Leaves Attenuate Inflammation via NF-κB Signaling and NLRP3 Inflammasome Activity in Macrophages. *Biomolecules* **2021**, *11*, 105.
10. Ratanachamnong, P.; Chunchaowarit, Y.; Namchaiw, P.; Niwaspragrit, C.; Rattanacheeworn, P.; Jaisin, Y. HPLC analysis and *in vitro* antioxidant mediated through cell migration effect of *C. hystrix* water extract on human keratinocytes and fibroblasts. *Heliyon* **2023**, *9*, 13068.
11. Abirami, A.; Nagarani, G.; Siddhuraju, P. *In vitro* antioxidant, anti-diabetic, cholinesterase and tyrosinase inhibitory potential of fresh juice from Citrus hystrix and C. maxima fruits. *Food Sci Hum Wellness* **2014**, *3*, 16-25.
12. Srifuengfung, S.; Bunyapraphatsara, N.; Satitpatipan, V.; Tribuddharat, C.; Junyaprasert, V.B.; Tungrugsasut, W.; Srisukh, V. Antibacterial oral sprays from kaffir lime (*Citrus hystrix* DC.) fruit peel oil and leaf oil and their activities against respiratory tract pathogens. *J Tradit Complement Med* **2020**, *10*, 594-598.
13. Sreepian, P.M.; Rattanasinganchan, P.; Sreepian, A. Antibacterial efficacy of *Citrus hystrix* (makrut lime) essential oil against clinical multidrug-resistant methicillin-resistant and methicillin-susceptible *Staphylococcus aureus* isolates. *Saudi Pharm J* **2023**, *31*, 1094-1103.
14. Tunjung, W.A.S.; Cinatl, J.; Michaelis, M.; Smales, C.M. Anti-Cancer Effect of Kaffir Lime (*Citrus Hystrix* DC) Leaf Extract in Cervical Cancer and Neuroblastoma Cell Lines. *Procedia Chem* **2015**, *14*, 465-468.
15. Ho, Y.; Suphrom, N.; Daowtak, K.; Potup, P.; Thongsri, Y.; Usuwanthim, K. Anticancer Effect of *Citrus hystrix* DC. Leaf Extract and Its Bioactive Constituents Citronellol and, Citronellal on the Triple Negative Breast Cancer MDA-MB-231 Cell Line. *Pharmaceuticals* **2020**, *13*, 476.

16. Abolmaesoomi, M.; Mat Junit, S.; Mohd Ali, J.; Chik, Z.B.; Abdul Aziz, A. Effects of polyphenolic-rich extracts from Citrus hystrix on proliferation and oxidative stress in breast and colorectal cancer. *Turk Biyokim Derg* **2023**, *48*, 110-118.
17. Abirami, A.; Nagarani, G.; Siddhuraju, P. Hepatoprotective effect of leaf extracts from Citrus hystrix and C. maxima against paracetamol induced liver injury in rats. *Food Sci Hum Wellness* **2015**, *4*, 35-41.
18. Buakaew, W.; Pankla Sranujit, R.; Noysang, C.; Krobthong, S.; Yingchutrakul, Y.; Thongsri, Y.; Potup, P.; Daowtak, K.; Usuwanthim, K. Proteomic Analysis Reveals Proteins Involved in the Mode of Action of β-Citronellol Identified From *Citrus hystrix* DC. Leaf Against *Candida albicans*. *Front Microbiol* **2022**, *13*, 894637.
19. Rao, X.; Huang, X.; Zhou, Z.; Lin, X. An improvement of the 2 -ΔΔCT method for quantitative real-time polymerase chain reaction data analysis. *Biostat Bioinforma Biomath* **2013**, *3*, 71-85.
20. Robert, S.; Gicquel, T.; Bodin, A.; Lagente, V.; Boichot, E. Characterization of the MMP/TIMP Imbalance and Collagen Production Induced by IL-1β or TNF-α Release from Human Hepatic Stellate Cells. *PLoS One* **2016**, *11*, 153118.
21. Krobthong, S.; Yingchutrakul, Y.; Samutrtai, P.; Hitakarun, A.; Siripattanapipong, S.; Leelayoova, S.; Mungthin, M.; Choowongkomon, K. Utilizing Quantitative Proteomics to Identify Species-Specific Protein Therapeutic Targets for the Treatment of Leishmaniasis. *ACS Omega* **2022**, *7*, 12580-12588.
22. Griss, J.; Viteri, G.; Sidiropoulos, K.; Nguyen, V.; Fabregat, A.; Hermjakob, H. ReactomeGSA - Efficient Multi-Omics Comparative Pathway Analysis. *Mol Cell Proteomics* **2020**, *19*, 2115-2125.
23. Berman, H.M.; Westbrook, J.; Feng, Z.; Gilliland, G.; Bhat, T.N.; Weissig, H.; Shindyalov, I.N.; Bourne, P.E. The Protein Data Bank. *Nucleic Acids Res* **2000**, *28*, 235-242.
24. Berman, H.; Henrick, K.; Nakamura, H. Announcing the worldwide Protein Data Bank. *Nat Struct Mol Biol* **2003**, *10*, 980-980.
25. Kim, S.; Chen, J.; Cheng, T.; Gindulyte, A.; He, J.; He, S.; Li, Q.; Shoemaker, B.A.; Thiessen, P.A.; Yu, B.; et al. PubChem 2023 update. *Nucleic Acids Res* **2023**, *51*, 1373-1380.
26. Liu, Y.; Yang, X.; Gan, J.; Chen, S.; Xiao, Z.-X.; Cao, Y. CB-Dock2: improved protein–ligand blind docking by integrating cavity detection, docking and homologous template fitting. *Nucleic Acids Res* **2022**, *50*, 159-164.
27. Pettersen, E.F.; Goddard, T.D.; Huang, C.C.; Couch, G.S.; Greenblatt, D.M.; Meng, E.C.; Ferrin, T.E. UCSF Chimera—A visualization system for exploratory research and analysis. *J Comput Chem* **2004**, *25*, 1605-1612.
28. Dewidar, B.; Meyer, C.; Dooley, S.; Meindl, B.; Nadja. TGF-β in Hepatic Stellate Cell Activation and Liver Fibrogenesis—Updated 2019. *Cells* **2019**, *8*, 1419.
29. Zhang, D.; Zhang, Y.; Sun, B. The Molecular Mechanisms of Liver Fibrosis and Its Potential Therapy in Application. *Int J Mol Sci* **2022**, *23*, 12572.
30. Westenberger, G., Sellers, J., Fernando, S., Junkins, S., Han, S. M., Min, K., & Lawan, A. Function of Mitogen-Activated Protein Kinases in Hepatic Inflammation. *J Cell Signal* **2021**, *2*, 172-180.
31. Darling, T.K.; Lamb, T.J. Emerging Roles for Eph Receptors and Ephrin Ligands in Immunity. *Front Immunol* **2019**, *10*, 1473.
32. Mekala, S.; Dugam, P.; Das, A. Ephrin–Eph receptor tyrosine kinases for potential therapeutics against hepatic pathologies. *J Cell Commun Signal* **2023**, *17*, 549-561.
33. Creeden, J.F.; Kipp, Z.A.; Xu, M.; Flight, R.M.; Moseley, H.N.B.; Martinez, G.J.; Lee, W.H.; Alganem, K.; Imami, A.S.; McMullen, M.R.; et al. Hepatic kinome atlas: An in-depth identification of kinase pathways in liver fibrosis of humans and rodents. *Hepatology* **2022**, *76*, 1376-1388.